On the Isotropy of the Dynamic Mechanical and Failure Properties of Swaged Tungsten Heavy Alloys

D. RITTEL, R. LEVIN, and A. DOROGOY

The quasi-static and dynamic mechanical and failure properties of a swaged tungsten-base heavy alloy rod have been investigated, with emphasis on the orientation of the specimens in the rod. Three orientations were considered, 0, 45, and 90 deg, with respect to the longitudinal axis of the rod. Compression, tension, and dominant shear tests were carried out. With the exception of the 0 deg orientation, all the orientations displayed quite similar mechanical characteristics in tension and compression. Dynamic shear revealed a critical strain for adiabatic shear failure of $\varepsilon_c \approx 0.13$, independent of the orientation and quite inferior to the quasi-static ductility. The present study confirms previous results obtained for one (generally unspecified) orientation and extends them to three orientations. Failure mechanisms were thoroughly characterized and it appears that significant damage does not develop prior to final failure. It is concluded that, for practical purposes, the swaged heavy alloy considered here can be regarded as *isotropic* from a mechanical and failure point of view, in spite of its microstructural anisotropy resulting from the swaging process.

I. INTRODUCTION

THE alloys referred to as "heavy alloys" generally consist of the alloy families containing elements of very high density, such as W, Ta, and U. Tungsten-base heavy alloys are produced by liquid-phase sintering of elemental powders, W, Ni, and Fe. The high density of these materials (typically in excess of 17 Mg/m^3) makes these alloys suitable for armor piecing purposes (kinetic penetrators).[1,14] The typical microstructure of a tungsten-base heavy alloy consists of nearly spherical single crystals of tungsten (bcc) surrounded by a binding phase (fcc matrix), which is a solid solution of W, Ni, and Fe. The mechanical properties of these alloys have been extensively studied, both quasi-statically (*e.g.*, References 2 through 5) and dynamically (*e.g.*, References 6 through 12), most recently in the examination of the alloy's ability to undergo shear localization in the form of adiabatic shear banding.[8–11] These heavy alloys can be produced in a variety of near-final shapes, but cylindrical rods are the most commonly produced. Various thermomechanical treatments are used to improve the properties of the rods, with swaging operations being the most common, to obtain the final desired cylindrical rod shape. Past research has shown that heavy alloys are strain-rate sensitive.[9,10] At low strain rates, the material exhibits some strain hardening that disappears gradually as the strain rate is increased ($\dot{\varepsilon} \approx 10^3 s^{-1}$). As the strain rate increases further, strain softening starts to occur, possibly due to the increase in local temperature and thermomechanical coupling effects.[5] When the components of the composite material are considered individually, they have different characteristics in terms of their high strain-rate behavior. A lack of strain hardening has been reported for dynamically loaded and cold-worked pure tungsten.[6] In addition, dynamic strain softening of textured tungsten has also been reported for the <001> orientation.[13] Zhou and Clifton[11] tested an alloy whose composition is representative of the binding matrix, and they observed no high strain rate related softening effects. All of the studies report that tungsten heavy alloys will ultimately fail at high strain rates through a mechanism involving adiabatic shear bands, first modeled by Zhou *et al.*[10] Ramesh[9] reports a critical shear strain to failure of $\gamma_c = 0.08$ to 0.13, while Zhou and Clifton report much higher values of $\gamma_c = 1$ to 1.5. For the most part, none of the previous studies have investigated the possible contribution of anisotropy to the mechanical properties and the resulting adiabatic shear band formation. The issue of adiabatic shear band formation has not been related to material orientation, even if the ballistic efficiency of the material depends on its tendency to fail by this mechanism. Weisbrod and Rittel[15,16] did study the anisotropy of the quasi-static and dynamic fracture properties of a tungsten-based heavy alloy and reported a significant anisotropy of the fracture toughness (quasi-static and dynamic). However, no extensive study has been performed on the relationship between material orientation and adiabatic shear band formation. In this study, a careful investigation was performed to address this issue using a 90:7:3 wt pct W/Fe/Ni alloy that had been swaged 25 pct. Three orientations (0, 45, and 90 deg to the longitudinal axis) were tested statically and dynamically in tension and in compression. In addition, a newly developed specimen, the shear compression specimen (SCS), was used to evaluate the response of the material in shear dominant deformation.[17,18,19]

The remainder of the article is organized as follows. Section II introduces the material, experimental specimens, and procedures, detailing the SCS. Section III starts with selected basic numerical results about the SCS, followed by the various mechanical characteristics measured. Section IV describes the specific failure micromechanisms of the investigated alloy. Section V summarizes and discusses the main results of this work, and Section VI provides concluding remarks.

D. RITTEL, Professor, and R. LEVIN and A. DOROGOY, Doctors, are with the Faculty of Mechanical Engineering, Technion Mechanical Engineering, Israel Institute of Technology, 32000 Haifa, Israel. Contact e-mail: merittel@technion.ac.il

Manuscript submitted February 24, 2004.

II. EXPERIMENTAL

A. *Material*

The material investigated in this work is a tungsten-iron-nickel alloy, of weight ratio 90:7:3. The material was liquid-phase sintered as a cylindrical rod. It was heat treated using proprietary treatments, and subsequently 25 pct swaged to a final diameter of 26 mm. The specimens were subsequently machined from the rod and supplied for the present study.

B. *Specimens*

The experimental specimens were machined in three selected orientations, 0 deg, 45 deg, and 90 deg, with respect to the longitudinal axis of the original rod. The specimens, their dimensions, and their denomination are shown in Figure 1. As shown in this figure, the specimens were essentially machined from the central part of the rod. Compression specimens are basically cylindrical specimens, whereas the tensile specimens are short, threaded specimens. A total of 14 and 6 specimens per orientation were tested in compression and tension, respectively. The small size of the specimens is dictated by the final diameter of the rod. Parallelepiped SCSs[17,18,19] were machined with their 45 deg slot oriented along each of the aforementioned directions. Three slot (gage) widths per orientation were selected: 2.5, 1, and 0.25 mm. Five specimens of each gage width were tested per orientation. The notch root radius was 0.2 mm for the wider gages and of the order of 0.1 mm for the 0.25-mm gage.

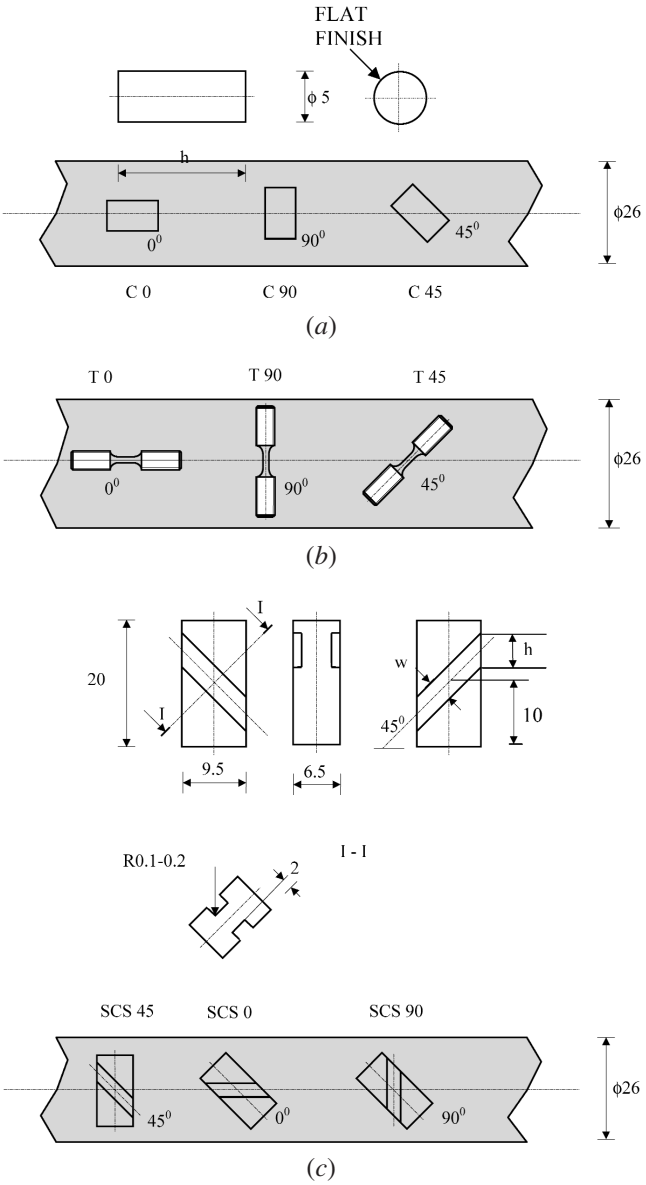

Fig. 1—Experimental specimens: (*a*) compression, (*b*) tension, and (*c*) shear compression (SCS).

C. *Testing*

Static compression and tension tests were performed on a servohydraulic, computer-controlled MTS 810 machine under displacement control. Tensile specimens were instrumented with a clip-on extensometer. Compression tests were carried out by inserting the cylinder between two hard steel flat platens lubricated with petroleum jelly. The same procedure was applied to quasi-stating testing of the SCS. In all the cases, the machine compliance was determined prior to testing, to improve the accuracy of the stress-strain diagrams.

Dynamic testing was carried out on a split Hopkinson pressure bar (Kolsky apparatus[20]). The diameter of the bars was 12.7 mm, and they were made of a similar tungsten-base heavy alloy. Geometric dispersion of the measured signals was accounted for and corrected using Lifshitz and Leber's algorithm.[21] Both cylindrical and SCS specimens were tested with this setup. Dynamic tension was performed on a modified Kolsky tension bar, 12.7 mm in diameter, made of 17-4 PH steel. Here, too, dispersion corrections were applied to the signals.

Characterization of the failure mechanisms was achieved first through scanning electron microscopy (SEM) fractographic analysis. In addition, longitudinal sections were prepared by sectioning Ni plated fracture surfaces at midthickness of the gage. Such longitudinal sections allow assessment of the nature and extent of the damaged zone below the main fracture surface, all along the crack path.

III. RESULTS

A. *Numerical Modeling of the SCS[23]*

Previous work with the SCS[17–19,23] has shown that the (Von Mises) equivalent stress, $\hat{\sigma}_{\text{eqv}}$, and strain, $\hat{\varepsilon}_{\text{eqv}}$, can be related to the applied load and specimen geometry by the following simple formulas:

$$\hat{\sigma}_{\text{eqv}} = k_1 (1 - k_2 \hat{\varepsilon}_{\text{eqv}}) \frac{P}{Dt} \qquad [1]$$

and

$$\hat{\varepsilon}_{\text{eqv}} = k_3 \frac{d}{h}; \dot{\hat{\varepsilon}}_{\text{eqv}} = k_3 \frac{\dot{d}}{h} \qquad [2]$$

where P is the applied load, d the prescribed displacement, D the specimen width, t the thickness of the gage, and $h = 1.414w$ its height. The coefficients k_1, k_2, and k_3 must be determined numerically, and are generally observed to be dependent

on both the material (*via* its hardening modulus) and the gage height, *h.* A finite-element model of the SCS was generated and solved using the ANSYS finite-element package.[22] Bilinear material behavior was assumed and the elastic-plastic problem was solved, allowing for geometrical nonlinearities by using a large strain formulation. Young's and tangent moduli, as well as the yield strength of the various orientations, were determined from the tensile and compressive tests. Both $\hat{\sigma}_{eqv}$ and $\hat{\varepsilon}_{eqv}$ were calculated by averaging the results on a midsection of the specimen gage. The boundary conditions consisted of a prescribed (negative) vertical displacement, while one node on the bottom face of the specimen was fully constrained. Determination of the k_i consisted of calculating the resultant load-displacement curve as a result of the prescribed displacement for a given material with assumed bilinear behavior. Earlier work showed that the calculated averaged $\hat{\sigma}_{eqv} - \sqrt{b^2 - 4ac_{eqv}}$ curve on a midsection of the gage accurately reproduced the assumed bilinear constitutive law.[23] P-$\hat{\varepsilon}_{eqv}$ and d-$\hat{\varepsilon}_{eqv}$ relations were thus identified using polynomial regressions, according to Eqs. [1] and [2]. A set of k_i was determined for each orientation and gage width, as summarized in Table I. The analyses clearly showed that all three orientations could be characterized by similar coefficients k_i for a given gage width.

As will be shown in the sequel, the validation of the overall approach, as shown in previous works[16,17,18] lies in the requirement that the equivalent stress-strain curve obtained using the SCS be similar to that obtained either through tension or compression tests, although the latter are limited in the range of strains attainable.

B. *Quasi-Static and Dynamic Compression*

Typical quasi-static compression stress-strain curves are shown for the three orientations in Figure 2. This figure shows that the material exhibits similar moderate strain hardening in all orientations, and that the 0 deg orientation is weaker than the other two orientations. Typical dynamic stress-strain curves are shown in Figure 3. Here, too, the 0 deg orientation appears to be weaker. Comparing Figures 2 and 3 shows the characteristic strain-rate sensitivity[6–13] together with a noticeable decrease in strain hardening, turning the material into elastic-almost perfectly plastic at high rates.

C. *Quasi-Static and Dynamic Tension*

As shown in Figure 4, the typical quasi-static tensile behavior is rather similar for all the orientations. The attainable range of strains is quite limited (about 0.03) as the specimens tend to neck early during deformation. Up to this strain level, strain hardening is moderate. Table II summarizes the various values of the Young's modulus measured in the quasi-static tensile tests.

Figure 5 shows characteristic dynamic stress-strain curves. All the tests reveal a similar initial inertial peak that stems

Table I. Coefficients for the SCS

w	k_1	k_2	k_3
0.3 mm	0.861	0.152	0.213
1.0 mm	0.927	0.219	0.628
2.5 mm	0.955	0.276	0.931

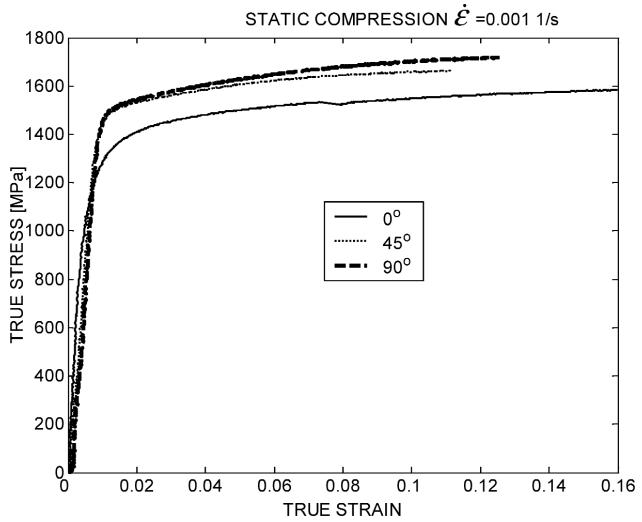

Fig. 2—Quasi-static compression. Typical true stress-strain curves for each orientation.

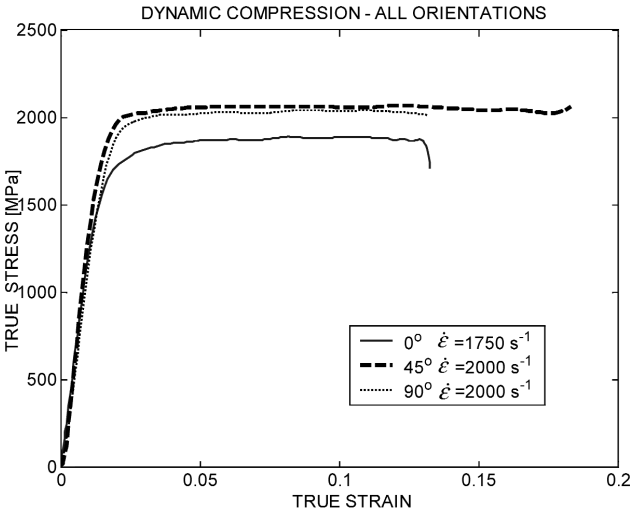

Fig. 3—Dynamic compression. Typical true stress-strain curves for each orientation.

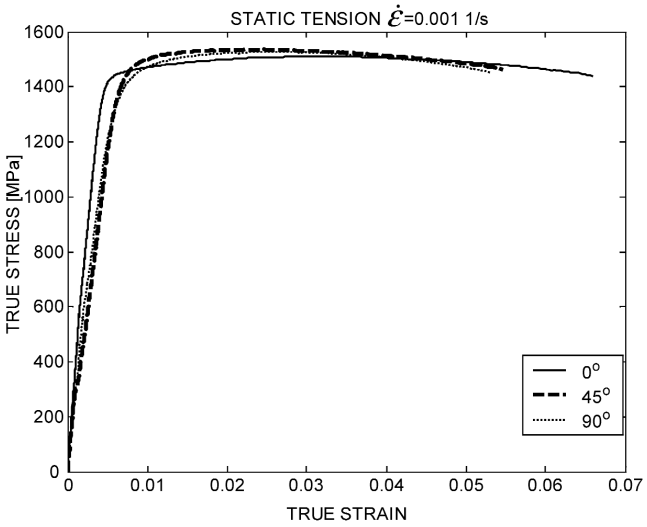

Fig. 4—Quasi-static tension. Typical true stress-strain curves for each orientation.

Table II. Young's Modulus—Quasi-Static Tension

	0 Deg	45 Deg	90 Deg
E (GPa)	≈347	≈350	≈361

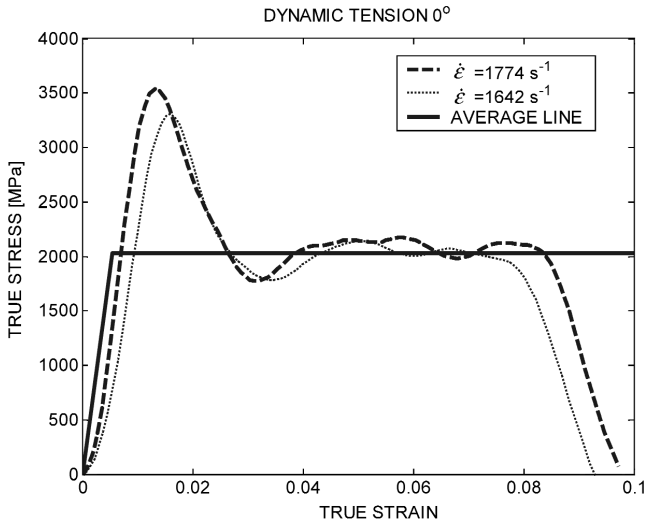

(*a*)

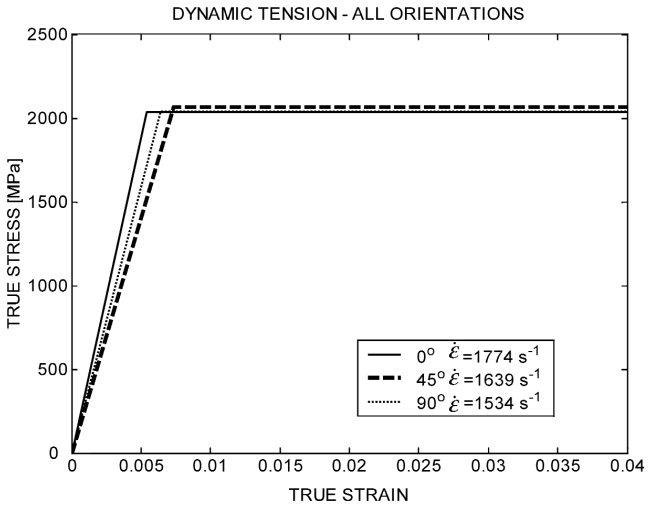

(*b*)

Fig. 5—Dynamic tension. (*a*) Typical true stress-strain curves for 0 deg orientation. Note the initial inertial peak and the bilinear approximation. (*b*) Typical true stress-strain curves for each orientation.

from lack of equilibrium across the specimen (Figure 5(a) for the 0 deg orientation). Figure 5(b) shows smoothed stress-strain curves for all three orientations together, without the inertial peak. This figure reveals similar characteristics, *i.e.,* almost perfect plastic flow and similar strength levels. Once again, one may note the marked strain-rate sensitivity of the material. Moreover, contrary to the compression tests, tension tests (static and dynamic) do not show a weaker orientation in this material.

D. *Quasi-Static and Dynamic Shear Compression Testing*

A distinctive feature of the SCS is that the deformation of the gage is dominated by shear, even if it is not pure

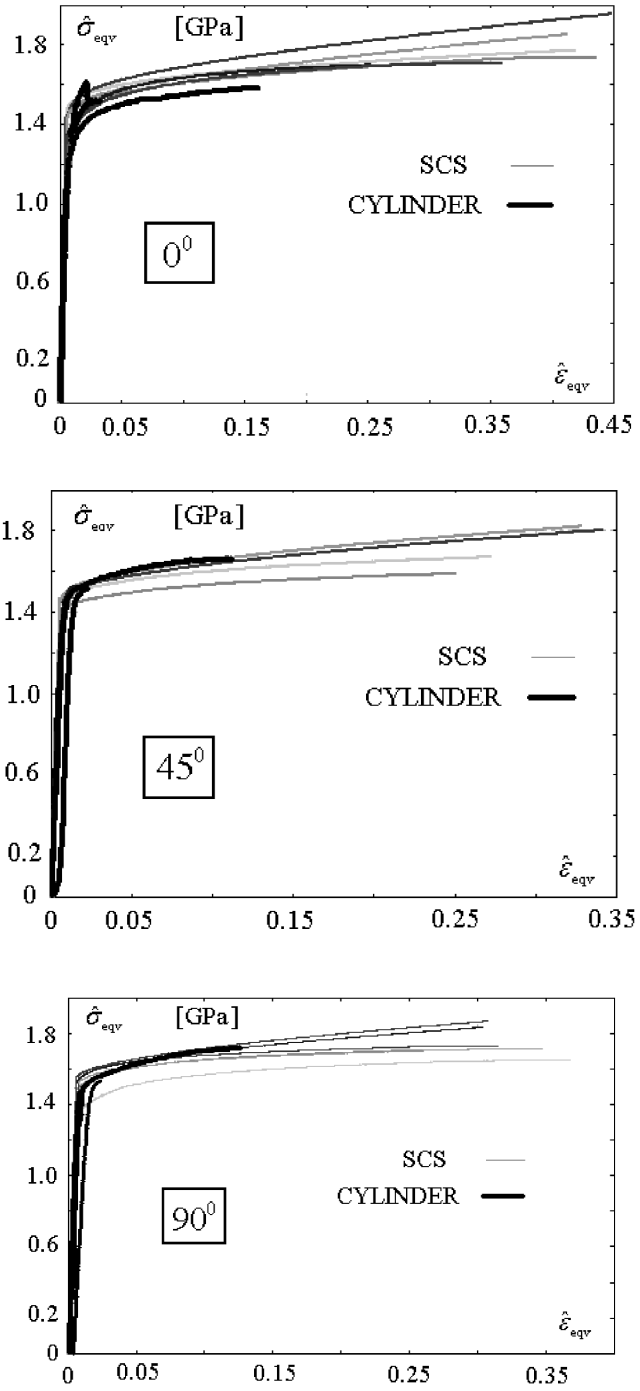

Fig. 6—Quasi-static shear compression tests. True stress-strain curves obtained for each orientation from cylindrical specimens and from SCSs. Note the high similarity of the results while larger strains are attainable with the SCS.

shear, as mentioned in Section I. Moreover, because of its geometry, the gage section does not neck or barrel markedly so that large strains can develop without problems, over a variety of strain rates. Figure 6 shows the typical $\hat{\sigma}_{eqv} - \hat{\varepsilon}_{eqv}$ curves for the SCSs, along with the curves obtained from tensile specimens. The high similarity between the two types of results validates the choice of the k_i coefficients. Here,

large strains of the order of 0.35 and greater are obtained, and the strain hardening capacity of the material is evident. It should be emphasized here that the specimens did not fracture at these strain levels because the test was interrupted arbitrarily. Therefore, a greater ductility can be expected for those tests shown in Figure 6.

Equations [1] and [2] are also applicable to dynamic testing, and characteristic results are shown in Figure 7. At high strain rates, the material again shows a lack of strain hardening and noticeable strain-rate sensitivity, as expected. In addition, a certain degree of softening can be noted past $\varepsilon = 0.1$ for those specimens whose testing ended by fracture, as shown in Figure 7. We observed that all the failed specimens fractured at an overall strain of $\varepsilon_c \approx 0.13$, as manifested by the unloading part of the stress-strain curve that does not unload parallel to the "elastic" part. It should be emphasized that the dynamic failure strain is considerably smaller that its quasi-static counterpart.

In these experiments, the yield stress could not be accurately determined using extensometric techniques. Consequently, we report values of the proportional stress, which corresponds to the end of the proportional stress-strain domain. The proportional stress gives an estimate of the "macroscopic" yield stress of the material. Table III summarizes typical proportional stress data for each orientation and test.

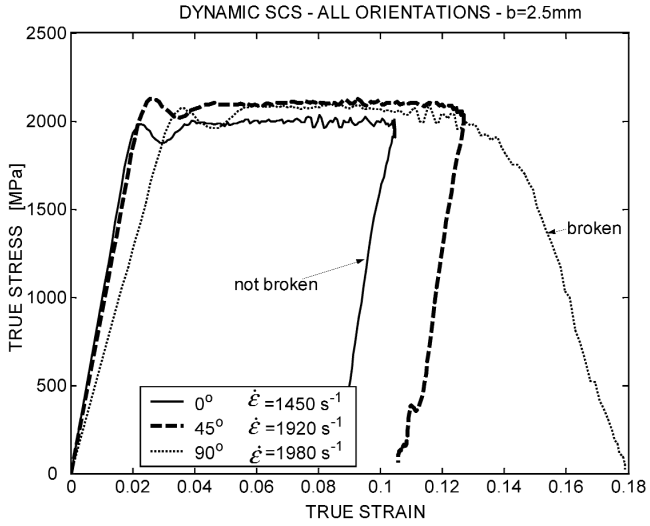

Fig. 7—Dynamic shear compression tests. Typical true stress-strain curves for each orientation. The 90 deg specimen fractured, as evidenced from the unloading part of the graph.

Table III. Summary of Characteristic Proportional Limits

Proportional Limit (MPa)	0 Deg	45 Deg	90 Deg
Quasi-static compression	≈1250	≈1500	≈1500
Dynamic compression	≈1750	≈2000	≈2000
Quasi-static tension	≈1450	≈1500	≈1500
Dynamic tension	≈2000	≈2000	≈2000
Quasi-static shear (SCS)	≈1500	≈1500	≈1500
Dynamic shear (SCS)	≈2000	≈2000	≈2000

E. *Failure Mechanisms*

1. *Tension tests*

Figures 8(a) through (c) show the failure micromechanisms of the quasi-static tensile specimen of each orientation.

For the 0 deg specimens, the fracture surface comprises essentially cleavage of the W grains with little evidence of ductile matrix failure. This is confirmed by observing the various profiles showing cleavage of the W grains and some matrix decohesion.

For the 45 deg specimens, one distinguishes cleavage, interfacial (binding necks) failure, and little matrix deformation. The profiles indicate the same mechanisms, but also reveal multiple cleavage cracks in a single W grain.

For the 90 deg specimens, the preceding failure mechanisms are complemented by evidence of ductile matrix failure (dimples). The profiles show that matrix failure occurs on the fracture surface only, as no damage is detected below it. Here, too, multiple W grain cleavage is observed. Figures 9 (a) through (c) show the failure micromechanisms of a dynamic tensile specimen of each orientation.

For the 0 deg specimens, the fracture surface comprises cleavage of the W grains and abundant ductile matrix failure. This is confirmed by observing the various profiles that also show that matrix damage remains confined to the fracture surface.

For the 45 deg specimens, one distinguishes essentially interfacial (binding necks) failure and noticeable matrix deformation. The profiles indicate the same mechanisms, but also reveal that the matrix damage now extends below the main fracture plane.

For the 90 deg specimens, one can note cleavage and interfacial failure, as well as profuse matrix failure (dimples). The

Table IV. Summary of the Main Failure Mechanisms Observed for the Three Orientations

Orientation	Static Tension	Dynamic Tension	Static Shear	Dynamic Shear
0 Deg	cleavage W	cleavage W *superficial* matrix ductile failure	homogeneous deformation	localized shear essentially W grains no matrix damage
45 Deg	cleavage W multiple cleavage W-W failure	W-W failure *extended* matrix ductile failure	homogeneous deformation	localized shear essentially W grains no matrix damage
90 Deg	cleavage W multiple cleavage W-W failure superficial matrix ductile failure	cleavage W W-W failure *extended* matrix ductile failure	homogeneous deformation	localized shear essentially W grains no matrix damage

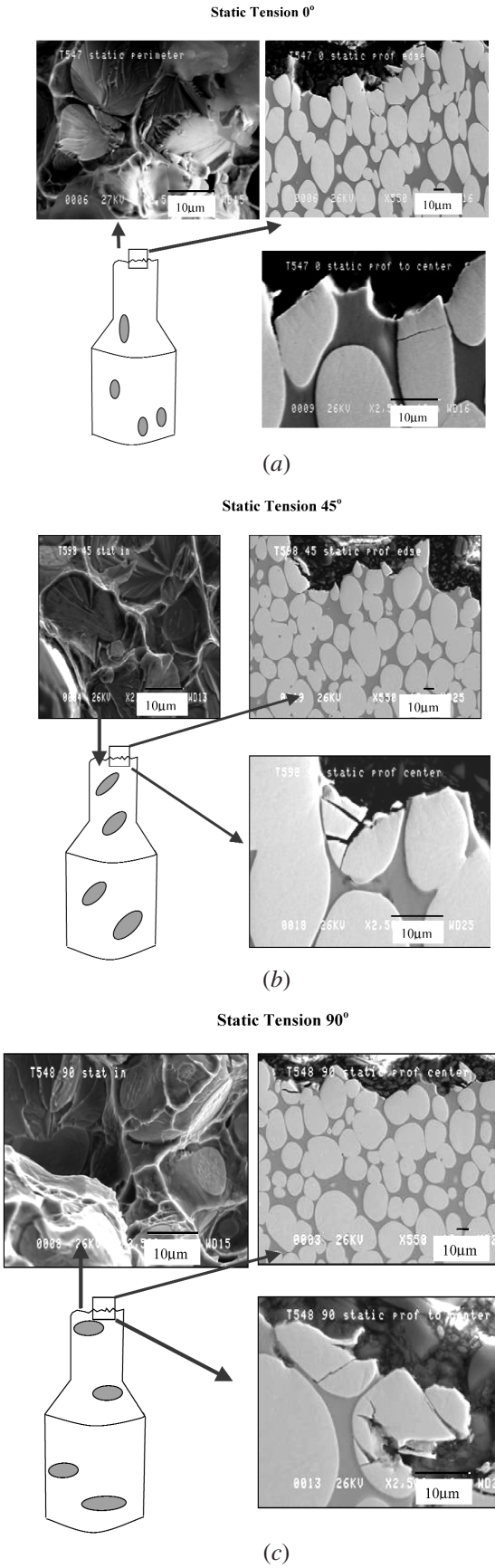

Fig. 8—Failure mechanisms of quasi-static tensile specimens at (*a*) 0 deg, (*b*) 45 deg, and (*c*) 90 deg. For each orientation, two longitudinal sections (perpendicular to the fracture plane) and one SEM fractograph are shown.

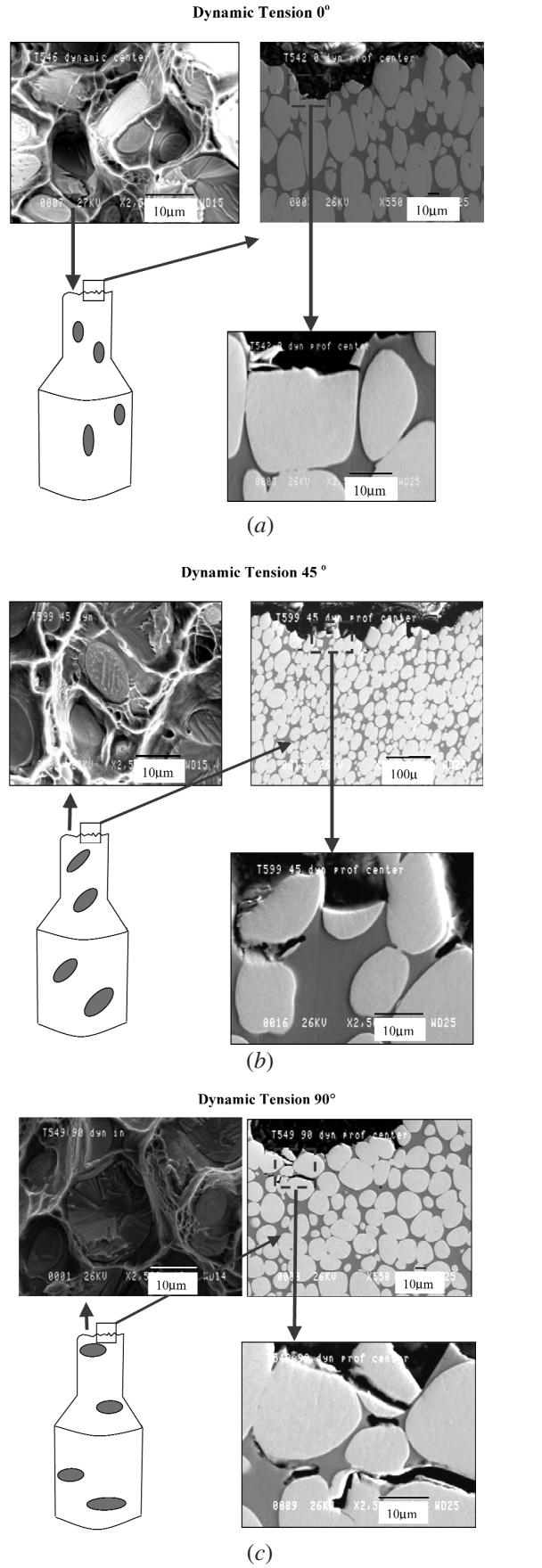

Fig. 9—Failure mechanisms of dynamic tensile specimens at (*a*) 0 deg, (*b*) 45 deg, and (*c*) 90 deg.

profiles indicate the same mechanisms, but also reveal that significant matrix damage extends below the main fracture plane.

2. *Shear dominant tests*

Quasi-static dominant shear is characterized in Figures 10(a) through (c) for orientations 0, 45, and 90 deg, respectively.

Here, we examined specimens that *did not fracture* after various levels of strain ($\varepsilon = 0.3$ to 0.45). In all cases, one can clearly see that the grains within the sheared gage rotate considerably with respect to those grains outside the gage. Moreover, these grains elongate noticeably without apparent damage in the adjacent matrix. These observations indicate a large ductility of the material when shear deformation is considered. All three orientations show identical response in this respect.

Dynamic dominant shear is characterized in Figures 11(a) through (c), for orientations 0, 45, and 90 deg, respectively. All specimens fractured, and we examined longitudinal midsections of the specimens, after having plated the fracture surface with Ni prior to sectioning.

All three orientations show an identical tendency to shear localization over a very small number of grains (typically less than five grains). This tendency is characterized by highly elongated tungsten grains that have undergone considerable deformation in the vicinity of the fracture surface. In this respect, all three directions respond identically in terms of shear localization under dynamic loading conditions, as was also noted from the mechanical characteristics. The interesting point is that we did not notice any significant damage, either at the tungsten-matrix interface or with the matrix itself, as was the case in some orientations for different loading conditions.

The fracture surfaces of the dynamically fractured SCSs all show similar features, regardless of the orientation. Severe wearing of the tungsten grains is observed, which indicates a high level of frictional stresses. This is characteristic of the shear failure mechanism, beyond which there is not much more to observe. A comparative summary of the failure micromechanisms is given in Table III (the reader is referred to Reference 24 for additional information on the failure mechanisms).

IV. DISCUSSION

The static and dynamic mechanical properties of a swaged tungsten-base heavy alloy have been systematically investigated, taking material orientation into account for the first time.

From a general point of view, the present results agree very well, and extend previous reports on the rate sensitivity of the material and its lack of strain hardening during dynamic deformation. These points were all noted for compression and torsion tests by Ramesh and co-workers.[8,9]

By contrast, the dynamic tensile behavior of these alloys has not been greatly investigated. Gero *et al.*[25] reported the operation of different failure mechanisms in quasi-static tension and compression. Specifically, these authors showed the role of the W-W interface in tension as opposed to the development of larger strains in both the matrix and the W grains in compression of the 0 deg orientation tested in the mentioned reference.[26] The present work does not address the failure mechanisms in compression, as the majority of the specimens did not fail during this test. However, the dynamic tensile failure mechanisms were observed to vary with the orientation of the specimen. This interesting observation complements partly Gero *et al.'s* observations in the

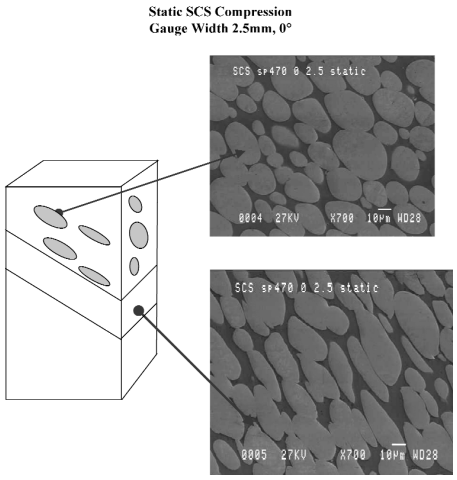

(*a*)

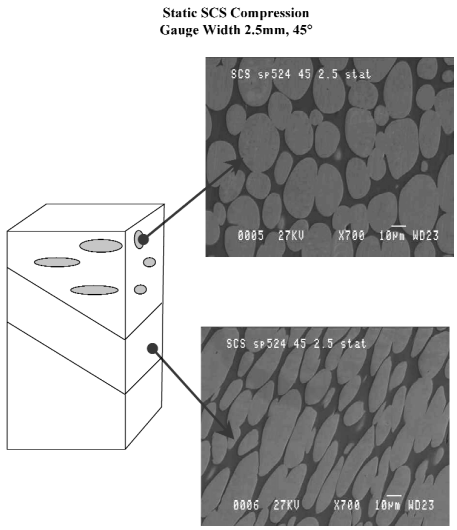

(*b*)

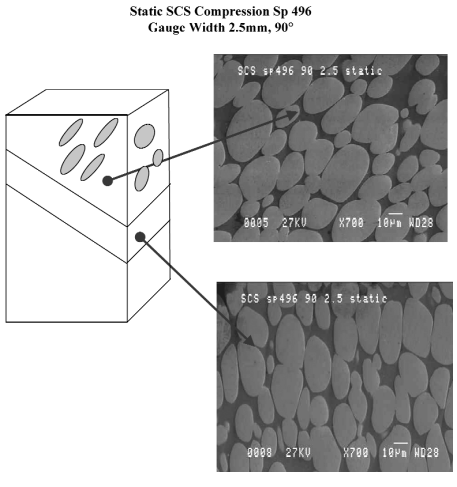

(*c*)

Fig. 10—Quasi-static SCS specimens. Longitudinal sections of deformed specimens that did not fracture at (*a*) 0 deg, $\varepsilon = 0.45$; (*b*) 45 deg, $\varepsilon = 0.35$; and (*c*) 90 deg, $\varepsilon = 0.30$. Note the grains' rotation and elongation within the gage section.

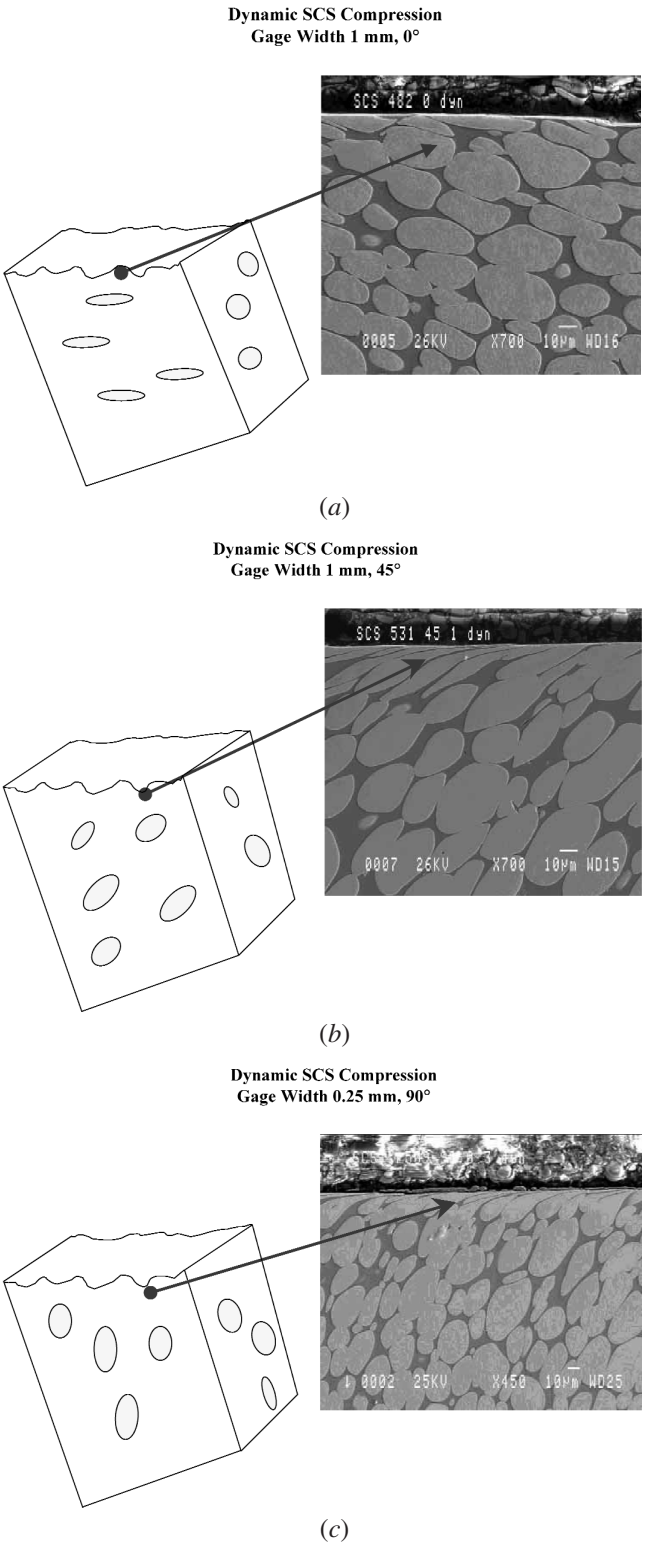

Fig. 11—Dynamic SCS specimens. Longitudinal sections of fractured specimens, perpendicular to the fracture surface, at (*a*) 0 deg, (*b*) 45 deg, and (*c*) 90 deg. It can be noted that the individual grains in the immediate vicinity of the fracture surface are heavily elongated and sheared.

sense that failure mechanisms in compression might be orientation dependent, as they are in tension.

The SCS test allows for the development of large strains, which are not usually attained with other tests. Due to the dominant state of shear, one can compare the results to those obtained using pure shear specimens[8] on the one hand. Yet, the concept of equivalent stress and strain also allows comparison with other uniaxial tests on the other hand. Numerical calculations and experimental observations have shown that the deformation is homogeneous with the specimen gage, as long as it does not become localized, as is the case for (adiabatic) shear band formation.[19,23] Having validated the numerical results pertaining to the data processing technique for the SCS, it is interesting to note that the static and dynamic shear responses of the material yield results that are comparable to those obtained with the other two testing techniques. Beyond the mere comparison of yield stress, it should be noted that the high rate SCS tests show some strain softening similar to that reported by Kim *et al.*[12] for their compression tests. Moreover, when compared with the shear tests of Ramesh,[9] our results show the very same trend for a dynamic failure strain that is noticeably smaller than its quasi-static counterpart. The present value of the failure strain, $\varepsilon_c \approx 0.13$, *i.e.,* $\gamma_c \approx 0.225$. This value is slightly higher than that reported by Ramesh[9] of $\gamma_c \approx 0.08$ to 0.13, and the difference may be due to differences in material composition and thermal treatments. However, the failure strain is considerably smaller than the value reported by Zhou and Clifton,[11] and one can tentatively relate this discrepancy to the very small specimen size used by these authors. Indeed, a thickness of 50 to 200 μm represents a small number of tungsten grains, so that a size effect may possibly influence the determination of the failure strain. Yet, one of the novelties of this work is that the observed value of the failure strain can now be extended to three main material orientations, thus showing an identical propensity to adiabatic shear failure in all three orientations. Therefore, to summarize the main results to this point, our results show that both the quasi-static and the dynamic mechanical properties of the investigated alloy are reasonably *isotropic,* thus generalizing previous observations. Moreover, the *failure characteristics,* mostly the dynamic ones, exhibit the same isotropy in terms of adiabatic shear band formation. These results are of prime importance when it comes to selecting an appropriate constitutive model and failure criterion for this material for numerical modeling purposes.

Yet, the very observation of an isotropic response for this swaged material contradicts all intuitive expectation. At this stage, one should discuss the deformation and failure mechanisms reported in this work. The failure mechanisms and their extent are distinct for each kind of test (static and dynamic) and orientation, to some extent. Comparing this observation with the observed isotropy of the mechanical response indicates that the failure mechanisms play no significant role during most of the deformation process. In other words, the various damage mechanisms that are observed after fracture, such as multiple cleavage of the W grains or interfacial decohesion at the W-matrix interface, all occur most likely very close to the final failure strain. The material does not undergo a significant level of damage during its plastic flow until near final failure. This point is further confirmed, *e.g.,* by the observations of the sheared, but unfractured longitudinal sections of the SCS, which all show significant plastic flow in the gage section without any appreciable sign of damage, whatever the orientation is. These same sections show a very high ductility of the composite (tungsten grains *and* matrix) as a whole regardless of the orientation. It is also interesting to note that the actual adiabatic shear failure zone is quite narrow (typically less than

5 W grains) and proceeds largely through a continuum of highly sheared W grains to a stage where the binding matrix is almost indiscernible. Again, the longitudinal sections through the fractured shear band do not reveal apparent signs of damage in the matrix or at the W matrix or W-W interfaces. This shows again that the various failure mechanisms all operate during final fracture of the specimen rather than developing gradually throughout the deformation process.

It should be noted in passing that this observation stands at odds with the qualification of "brittle material" that is very often found in the literature when the tungsten component of heavy alloys is mentioned. These particles are far from being brittle, as can be seen in all the micrographs shown here. The confusion arises most likely from the fact that the tungsten particles in the present alloy (and its likes) are single crystals that can exhibit considerable plastic flow, as opposed to polycrystalline tungsten.

Finally, it seems that material anisotropy should induce mechanical anisotropy, for both the mechanical and failure properties of the investigated material. The results presented in this study point to an apparent lack of such anisotropy, which may be stated in another way. Namely, there is certainly some anisotropy of the mechanical and failure properties; however, the experimental "resolution" of the present tests, along with the natural dispersion of the experimental results, did not allow for its observation, meaning that for engineering purposes, the investigated material can be considered as mechanically isotropic. This observation indicates that the 25 pct diameter reduction due to the swaging process does not induce anisotropy of the mechanical properties close to the center of the rod.

V. CONCLUSIONS

The influence of material anisotropy of a swaged tungsten-base heavy alloy on its mechanical and failure properties was examined for the first time, both quasi-statically and dynamically. Three orientations were tested in compression, tension, and shear dominant tests: 0, 45, and 90 deg with respect to the longitudinal axis of the swaged rod.

The main conclusions of the present study can be summarized as follows.

- The 0 deg orientation is weaker than the other two orientations in quasi-static and dynamic compression, in agreement with previous observations.[25] However, this difference is not observed for the other tests and all orientations exhibit quite similar mechanical properties.
- The investigated material is noticeably strain-rate sensitive in accordance with previous observations. At high strain rates, the strain hardening capacity vanishes, turning the material into elastic-almost ideally plastic. This result applies for all three orientations.
- The newly introduced SCS allows for development of large strains that are otherwise limited by mechanical instabilities. Quasi-static testing shows a high ductility for all three orientations where $\varepsilon > 0.35$.
- By contrast, all the failed SCSs fracture at an equivalent strain of $\varepsilon_c \approx 0.13$. This value is of the same order of magnitude as that reported by Ramesh,[9] and can, again, be generalized to all the orientations in question.
- Characteristic failure mechanisms have been identified for each test and orientation, using SEM metallographic and fractographic analysis.
- Little damage is identified below the main fracture plane. In all the tests and orientations, the material exhibits a high overall ductility for each of its components.
- A marked tendency for shear localization was observed for all the orientations, again with little damage. These observations indicate that the various damage and failure mechanisms all operate close to the final failure strain, rather than throughout the deformation process.
- Mechanical and failure anisotropy was not observed in the present work, possibly due to its small extent. This indicates the minor influence of the swaging process close to the rod's center.
- Therefore, for all practical purposes, the investigated swaged heavy alloy can be treated as mechanically isotropic.

ACKNOWLEDGMENTS

Financial support was provided through Grant No. 030-052. The Fund for Promotion of Research at Technion is acknowledged for partial support. The authors thank Drs. R. Gero, L.Boruchin, A. Pikus, and C. Weinberger for stimulating discussions.

REFERENCES

1. W.E. Gurwell, R.G. Nelson, G.B. Dudder, and N.C. Davis: PNL Report No. 218, PNL, Richland, WA.
2. R.H. Krock and L.A. Shepard: *Trans. TMS-AIME,* 1963, vol. 227, pp. 1127-34.
3. D. Rittel, I. Roman, and M. Bercovier: *ASME Trans., J. Eng. Mater. Technol.,* 1986, vol. 108, pp. 159-62.
4. D. Rittel and I. Roman: *Mater. Sci. Eng.,* 1986, vol. 82, pp. 93-99.
5. R.G. O'Donnell and R.L. Woddward: *Metall. Trans. A,* 1990, vol. 21A, pp. 744-48.
6. A.K. Zurek and G.T. Gray III: *J. Phys. IV Coll. C3,* 1991, vol. 1, pp. C3-631-C3-637.
7. H. Couque, J. Lankford, and A. Bose: *J. Phys. III France,* 1992, vol. 2, pp. 2225-38.
8. K.T. Ramesh and R.S. Coates: *Metall. Trans. A,* 1992, vol. 23A, pp. 2625-30.
9. K.T. Ramesh: *Mech. Mater.,* 1994, vol. 17, pp. 165-73.
10. M. Zhou, A. Needleman, and R.J. Clifton: *J. Mech. Phys. Solids,* 1994, vol. 42 (3), pp. 423-58.
11. M. Zhou and R.J. Clifton: *J. Appl. Mech.,* 1997, vol. 64, pp. 487-94.
12. D.S. Kim, S. Nemat-Nasser, J.B. Isaacs, and D. Lischer: *Mech. Mater.,* 1998, vol. 28, pp. 227-36.
13. G. Subhash, Y.J. Lee, and G. Ravichandran: *Acta Metall. Mater.,* 1994, vol. 42 (1), pp. 319-30.
14. L.S. Magness, Jr.: *Mech. Mater.,* 1994, vol. 17, pp. 147-54.
15. G. Weisbrod and D. Rittel: *Int. J. Fracture,* 2000, vol. 104 (1), pp. 91-104.
16. D. Rittel and G. Weisbrod: *Int. J. Fracture,* 2001, vol. 212, pp. 87-98.
17. D. Rittel, S. Lee, and G. Ravichandran: *Experim. Mech.,* 2002, vol. 42 (1), pp. 58-64.
18. D. Rittel, S. Lee, and G. Ravichandran: *Mech. Mater.,* 2002, vol. 34, pp. 627-42.
19. M. Vural, D. Rittel, and G. Ravichandran: *Metall. Mater. Trans. A,* 2003, vol. 34A (12), pp. 2873-85.
20. H. Kolsky: *P. Phys. Soc. London,* 1949, vol. 62B, pp. 676-700.
21. J.M. Lifshitz and H. Leber: *Int. J. Impact Eng.,* 1994, vol. 15 (6), pp. 723-33.
22. *ANSYS, User's Manual,* Ansys Inc., 2003.
23. A. Dorogoy and D. Rittel: *Int. J. Plasticity,* 2004.
24. R.G. O'Donnell and R.L. Woddward: *J. Mater. Sci.,* 2000, vol. 35, pp. 4319-24.
25. R. Gero, L. Borukhin, and I. Pikus: *Mater. Sci. Eng.,* 2001, vol. A302, pp. 162-67.
26. R. Gero, L. Borukhin, and I. Pikus: *private communication,* Ashot-Ashkelon, 2003.